On wings of minimal moments

Dominic Pearman*
*Freelance Electronics Developer, 88131 Lindau (Bodensee), Germany

Abstract

Optimisation of lifting surface span-loads using lifting-line theory has established the elliptic distribution to be ideal for given span while constraining weight generates solutions that reduce induced drag but incur span increases. This theoretical study extends the latter's theory to include moments of lift and of induced drag and investigates their characteristics in relation to the elliptic case. Evaluation for variable span determines reductions in moment of induced drag by up to 44 % and yields negative values in outboard regions of the span-wise distributions of both induced drag and its moment, corroborating experimentally observed proverse yaw. These results provide theoretical affirmation of suitably placed control surfaces potentially obviating dedicated yaw devices. Evaluation for given span leads to simultaneous increase in induced drag by up to 33% as well as decreases in moment of lift and of induced drag of up to 20 % and 33 %, respectively. The latter two results predict power reductions for driven rotors by minimising rotary moment instead of wake energy as well as noise abatement by lessening tip flow discontinuities.

Keywords

Lift distribution; lifting-line theory; moment; rotor blade; span-load; wing

1 INTRODUCTION

According to lifting-line theory, span-wise circulation distributions for lifting surfaces of given lift and span generate minimal drag when elliptic in shape [1] and have established themselves as default solutions for optimising wing designs. One consequence thereof is span-wise constant trailing edge downwash, which in turn causes adverse yaw and necessitates auxiliary yaw control devices to achieve controlled directional flight, usually in the form of rudders.

Proposals for non-elliptic distributions by setting wing lift and weight predict lower induced drag at the cost of span increases [2, 3]. Since their enhancements are surpassed by elliptic distributions of equivalent spans, they have received little attention or application to lifting surface implementations.

However, span-wise circulation distributions influence aerodynamic characteristics other than induced drag. Recent experimental observation of proverse yaw based on a bell-shaped distribution sets out the possibility of controlled directional flight without auxiliary yaw control devices and explains the absence of vertical tails on birds [4]. However, the study does not detail the arithmetic underpinnings necessary to create designs exploiting these findings.

This is taken as motivation to study the underlying mathematical models and build on the approach of setting lift together with its integrated moment instead of span to optimise aerodynamic wing characteristics as laid out in [2]. The theory presented therein is extended to deriving moments of force for both lift and induced drag. These are subsequently evaluated and results analysed with respect to ramifications for lifting surfaces and associated flight mechanics, in particular yaw.

Conventional rotor optimisation aims to minimise wake energy, which is achieved through constant flow acceleration across a rotor area [5, 6]. Therefore, individual blades are created so as to generate span-wise constant downwash, in striking similarity to lifting surfaces of elliptic span-loads. However, because the two investigated moments determine rotary moment, or torque, they are of greater relevance to rotating wings than their respective forces. Evaluation of non-elliptic distributions for given span is therefore examined with respect to implications for rotor blade applications.

The coordinate system used herein follows conventions of [1] that form the basis for [2] and is illustrated in Figure 1 with primary characteristics and their orientations. The wing surface lies in the xy-plane and moves along the y-axis, flow in positive or wing in negative direction.

The two moments being considered are moment of lift, M_L, acting perpendicular to the wing surface around its centreline, the y axis, and moment of induced drag, M_{Di}, in the plane of the wing around

doi: 10.25967/570033

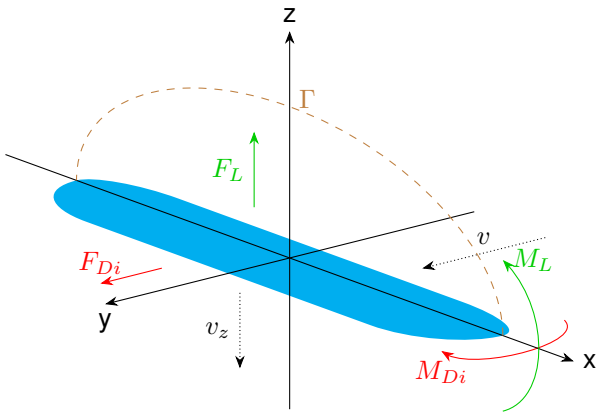

Figure 1: Coordinate system with primary characteristics

Software	Version
Python	3.10.5
Sympy	1.10.1

Table 1: Computational tools

the vertical z axis. Due to symmetry of the distribution functions about their respective axes of rotation, moments for each semi-span are equal and opposite, thereby canceling each other out to return zero for lifting surfaces as a whole. Therefore, it is only useful to derive moments of force for one semi-span acting at its root and not an entire symmetric wing.

Derivations and evaluations presented herein are performed using Python [7] and its symbolic mathematics library SymPy [8] in versions listed in Table 1.

2 LIFT DISTRIBUTIONS

2.1 Circulation, flow and induced drag

To generate non-elliptic span-loads, a circulation distribution factor ι is introduced as [2]

$$\iota = \frac{-\Gamma_2}{\Gamma_0}, \tag{1}$$

where Γ_0 and Γ_2 are the zeroth and second circulation components of the general solution proposed in [1] to determine optimal lift distributions. The symbol μ used in [2] is replaced by ι herein to avoid confusion with dynamic viscosity and the International System of Units (SI) prefix for micro. Span-wise circulation distributions are generated using ([2] eq. (5))

$$\Gamma = \Gamma_0 \cdot \sqrt{1-\xi^2}(1-\iota\xi^2), \tag{2}$$

where ξ is shorthand for the relative semi-span location $x/\frac{b}{2}$ and ranges from -1 to 1. An ι value of 0 generates elliptic distributions and the maximum useful value is 1. Equations are arranged so that terms involving the distribution factor evaluate to 1 for ι = 0. As the distribution function is the product of a term containing the root of a square, arguably of degree one, with a polynomial of degree two, the term 'cubic' is proposed to refer to distributions generated in this manner.

Central circulation Γ_0 is expressed as ([2] eq. (10))

$$\Gamma_0 = \frac{F_L}{\pi\rho \cdot r_{IM} \cdot v} \cdot \sqrt{\frac{1-\frac{\iota}{2}}{(1-\frac{\iota}{4})^3}}, \tag{3}$$

where F_L is lift, ρ density, v free-flow velocity and arm of integrated moment of lift, r_{IM} replacing r of the original equations, is determined by ([2] eq. (9))

$$b = 4 \cdot r_{IM} \cdot \sqrt{\frac{1-\frac{\iota}{4}}{1-\frac{\iota}{2}}}, \tag{4}$$

with b representing span. Vertical flow velocity at the trailing edge, v_z replacing w of the original equation to avoid confusion with weight, evaluates to ([2] eq. (6))

$$v_z = \frac{\Gamma_0}{2b} \cdot (1 + \frac{\iota}{2} - 3\iota\xi^2) \tag{5}$$

and is considered positive in the negative, downward z direction. Lift induced drag, F_{Di} replacing W of the original, is expressed as ([2] eq. (11))

$$F_{Di} = \frac{F_L^2}{8\pi\rho \cdot r_{IM}^2 \cdot v^2} \frac{(1-\frac{\iota}{2})(1-\frac{\iota}{2}+\frac{\iota^2}{4})}{(1-\frac{\iota}{4})^3}. \tag{6}$$

The derivation in [2] ends at this point and numerical results of central circulation Γ_0, span b and induced drag F_{Di} for ι of 0.00, 0.25, 0.50, 0.75 and 1.00 are presented and briefly discussed. A reduction in induced drag of up to 11.1 % at the cost of a span increase of up to 22.5 % is observed and appreciable impact of lower ι values is noted.

2.2 Moments of lift and of induced drag

Moment of force is defined as product of force and its arm so that moment of lift, M_L, is determined by integrating the product of circulation Γ, free-flow velocity v and semi-span location ξ over one semi-span to give

$$\begin{aligned} M_L &= \rho \cdot \int_0^1 \Gamma \cdot v \cdot \xi \, d\xi = \\ &= \frac{4 \cdot F_L \cdot r_{IM}}{3\pi} \frac{(1-\frac{2\iota}{5})}{\sqrt{(1-\frac{\iota}{2})(1-\frac{\iota}{4})}} \end{aligned} \tag{7}$$

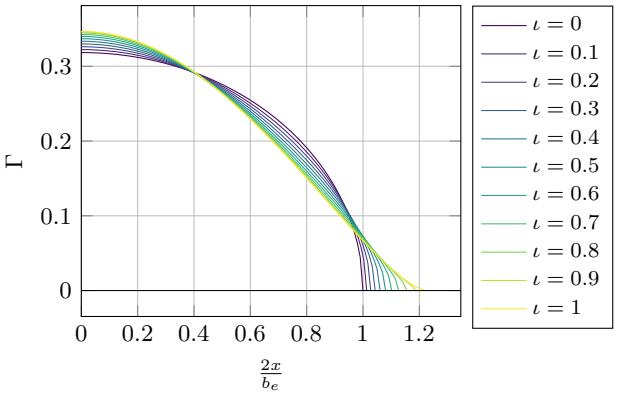

Figure 2: Circulation distribution for given lift and variable span

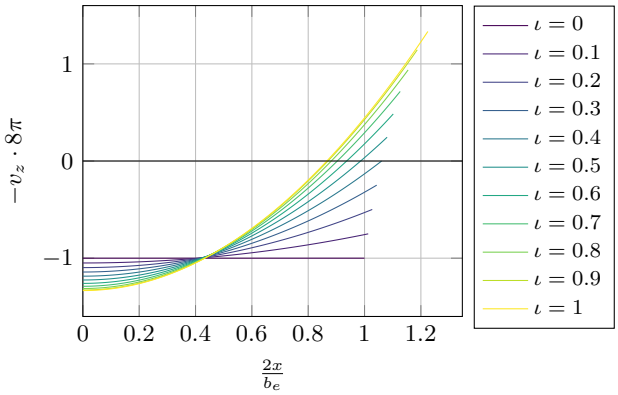

Figure 3: Trailing edge vertical flow distribution for given lift and variable span

Moment of induced drag, M_{Di}, is calculated by replacing free-flow velocity v with trailing edge vertical flow velocity v_z and performing the same integration to produce

$$M_{Di} = \rho \cdot \int_0^1 \Gamma \cdot v_z \cdot \xi \, d\xi = \\ = \frac{F_L^2}{6\pi^2 \rho \cdot r_{IM} \cdot v^2} \frac{(1 - \frac{11}{10}\iota + \frac{17}{35}\iota^2)\sqrt{1 - \frac{\iota}{2}}}{(1 - \frac{\iota}{4})^2 \sqrt{1 - \frac{\iota}{4}}} \tag{8}$$

It is to be noted that these equations pertain to the semi-span in the positive x direction and moments for the other side are opposed in sign and direction but equal in magnitude. Both are derived using SymPy's `integrate` function.

3 EVALUATION

3.1 Given lift, variable span

To investigate characteristics for given lift and its integrated moment while letting span vary as presented in [2], preceding equations are evaluated with lift F_L and radius of its integrated moment r_{IM} as well as ρ and v set to unitary values.

Span-wise plots of circulation Γ, trailing edge vertical flow velocity v_z, induced drag F_{Di} and moment of induced drag M_{Di} for one semi-span with these constraints are displayed in Figure 2, Figure 3, Figure 4 and Figure 5, respectively. In each case, curves for ι of 0 to 1 in steps of 0.1 are plotted in relation to the elliptic span b_e on the horizontal axis. Vertical axes are multiplied by constants as indicated to provide meaningful scales. The first two figures correspond to 'Abb. 1' in [2].

As distribution factor ι is incremented, circulation distributions exhibit three distinct regions of change. Circulation is raised in the innermost region up to ξ of about 0.4 while being successively lowered beyond and up to about 0.9 with a progressively linear slope. Beyond the elliptic span, additional regions of circulation are added which indicates the span extensions.

Overall, circulation is shifted from the middle region of each semi-span to its inner and outer sections, thereby maintaining constant integrated lift moment despite increases in span. In addition, differences between curves diminish, particularly for values of 0.8 to 1.0. The shape for ι = 1 has led to the common designation 'bell-shaped' and indicates that practical implementations involve pointed wing tips [2].

Trailing edge vertical flow distributions, plotted inverted in Figure 3 to illustrate proper orientation, feature several noteworthy characteristics. For the elliptic case (ι = 0), the span-wise distribution exhibits constant downward velocity, or downwash, along the entire span, since the second term of Equation 5 evaluates to 1 irrespective of ξ. Non-zero values of ι cause flow velocity along the span to to vary, forming upward parabolic shapes with progressively larger peak values at the centre and steeper slopes towards the tip. For ι up to 0.4, trailing edge flow remains entirely negative, i.e. downwash.

Above ι of 0.4, they begin to exhibit regions of upward flow in the outermost region with the point at which flow changes direction moving inwards and peak upwash velocities increasing as ι is raised. For these distributions, vortices no longer form at the tip, but rather underneath the wing, and velocity discontinuities at the tip disappear. For ι of 1, peak velocities at centreline and tip are equal in magnitude and opposite in orientation.

Being the product of preceding circulation and trailing edge vertical flow, induced drag distributions displayed in Figure 4 exhibit resultant features. Due to constant downwash, the drag distribution for ι = 0 matches the elliptic shape of its circulation distribution. As ι is raised up to 0.4, curves concentrate closer to the centreline with larger peak values while

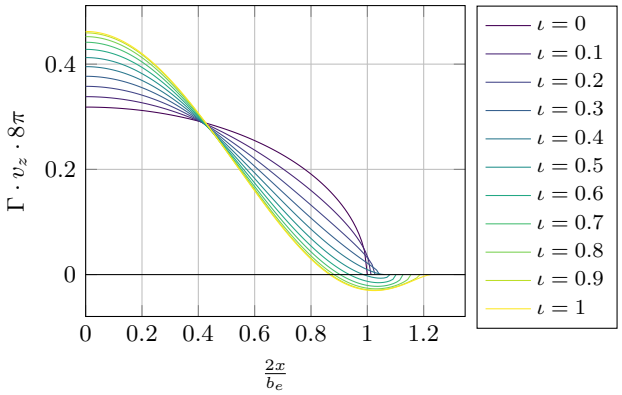

Figure 4: Induced drag distribution for given lift and variable span

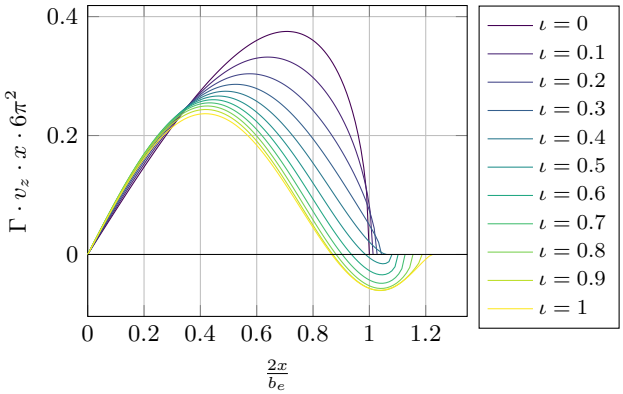

Figure 5: Induced moment distribution for given lift and variable span

remaining purely positive, i.e. drag, along the span.

For values above 0.4, progressive concentration of drag towards the centreline continues as ι is raised and small regions of negative induced drag appear towards the tip as a consequence of positive circulation combining with negative flow observed previously. Peak values, both positive and negative, are greatest for ι = 1 while variations between curves diminish for large distribution factors.

Span-wise distributions of moment of induced drag shown in Figure 5 depict subsequent decreases in maxima as well as areas under the respective curves as ι is raised. Up to ι of 0.4, values remain wholly positive.

For factors greater than 0.4, outer regions of negative drag cause corresponding negative moments, translating to orientation into oncoming flow, and are more pronounced due to their greater arm. As for previous characteristics, differences between curves for large distribution factors diminish, notably between 0.8 and 1.

Resultant total values for span b, induced drag F_{Di}, lift-to-drag ratio F_L/F_{Di} as well as moments of lift M_L

ι	b	r_{IM}	F_L	F_{Di}	F_L/F_{Di}	M_L	M_{Di}
0	1.000	1.000	1	1.000	1.000	1.000	1.000
0.1	1.013	1.000	1	0.976	1.024	0.998	0.929
0.2	1.027	1.000	1	0.955	1.047	0.995	0.862
0.3	1.043	1.000	1	0.937	1.067	0.992	0.800
0.4	1.061	1.000	1	0.922	1.085	0.990	0.742
0.5	1.080	1.000	1	0.910	1.099	0.988	0.691
0.6	1.102	1.000	1	0.901	1.111	0.985	0.647
0.7	1.127	1.000	1	0.894	1.118	0.983	0.610
0.8	1.155	1.000	1	0.891	1.123	0.982	0.583
0.9	1.187	1.000	1	0.889	1.125	0.980	0.566
1	1.225	1.000	1	0.889	1.125	0.980	0.560

Table 2: Normalised characteristics for given lift and variable span

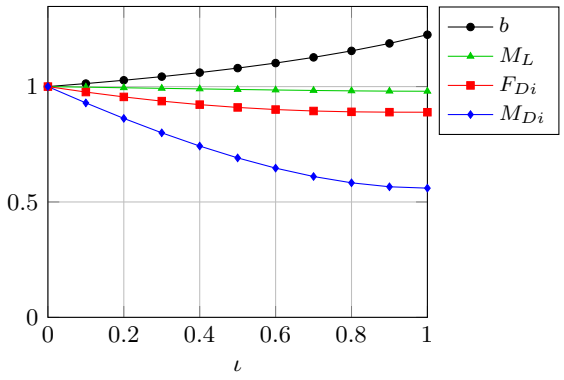

Figure 6: Variation of span, drag, moment of lift and of induced drag with distribution factor for variable span

and of induced drag M_{Di} normalised to the elliptic case are summarised in Table 2 and plotted versus distribution factor in Figure 6.

Span b increases continually by up to 22.5 % relative to the baseline elliptic case, as observable in distribution plots. Simultaneously. induced drag F_{Di} decreases by up to 11.1 %, estimable by the slight decreases in area under the curves of Figure 4 with increasing ι. These are results presented in 'Zahlentafel 1' of [2]. Most of the drop in induced drag occurs between ι of 0 and 0.6, for which a reduction of 9.9 % is observed. Beyond that, F_{Di} decreases by a further 1.2 % to a total of 11.1 % for ι of 0.9 to 1.0.

Consequently, lift-to-drag ratio F_L/F_{Di} improves by up to 12.5% with values for ι of 0.0 to 0.6 exceeding those of corresponding spans, but dropping below for larger factors.

Moment of lift M_L decreases marginally by up to 2 %, exemplifying the similarity of these results to those of [3] when setting it as the second optimisation constraint. The decrease is approximately linear up to an ι value of 0.9 and levels off thereafter.

At up to 44.0 %, the impact on moment of induced drag M_{Di} is far greater than any other considered characteristic, evidenced by the substantially smaller areas beneath curves in Figure 5 as ι is raised. This

ι	b	r_{IM}	F_L	F_{Di}	F_L/F_{Di}	M_L	M_{Di}
0	1.000	1.000	1	1.000	1.000	1.000	1.000
0.1	1.000	0.987	1	1.002	0.998	0.985	0.941
0.2	1.000	0.973	1	1.008	0.992	0.968	0.886
0.3	1.000	0.959	1	1.020	0.981	0.951	0.834
0.4	1.000	0.943	1	1.037	0.964	0.933	0.787
0.5	1.000	0.926	1	1.061	0.942	0.914	0.746
0.6	1.000	0.908	1	1.093	0.915	0.894	0.713
0.7	1.000	0.888	1	1.135	0.881	0.873	0.688
0.8	1.000	0.866	1	1.188	0.842	0.850	0.673
0.9	1.000	0.842	1	1.253	0.798	0.826	0.672
1	1.000	0.817	1	1.333	0.750	0.800	0.686

Table 3: Normalised characteristics for given lift and given span

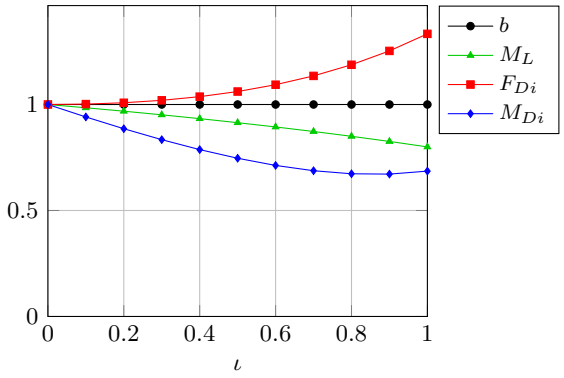

Figure 7: Variation of span, drag, moment of lift and of induced drag with lift distribution factor for given span

results from concentration of induced drag towards the centreline, steeper fall-off towards the outer wing and regions of negative drag at the tip. In a manner similar to induced drag, decreases are largest for small ι, though the leveling off beginning at 0.8 occurs at comparatively larger factors.

3.2 Given lift, given span

To investigate characteristics further, cubic lift distributions are evaluated setting lift and span as constraints, leaving integrated moment of lift variable. This is achieved by rearranging Equation 4 for r_{IM} given a set span b to return

$$r_{IM} = \frac{b}{4}\sqrt{\frac{1-\frac{\iota}{2}}{1-\frac{\iota}{4}}}. \tag{9}$$

Induced drag F_{Di}, lift-to-drag ratio F_L/F_{Di} as well as moment of lift M_L and of induced drag M_{Di} are subsequently evaluated by inserting r_{IM} from Equation 9 into Equation 6, Equation 7 and Equation 8 for given lift F_L and span b while varying lift distribution factor ι. Normalised characteristics are summarised in Table 3 and plotted in Figure 7.

Span-wise distributions of circulation, vertical flow velocity, induced drag and moment of induced drag retain qualitative features described for given lift and variable span but differ quantitatively in that peak values, both positive and negative, are greater and differences between curves for vaying ι are more pronounced. Little additional information may be gained from them, so they are not reproduced here and the focus is on normalised total values.

From results in Table 3 and plots in Figure 7 it is evident that the chosen constraints cause drops in integrated moment arm r_{IM} and moment of lift M_L of up to 18.3 % and 20.0 %, respectively. This is caused by greater concentration of circulation towards the centreline together with steeper slopes towards the tip as ι is raised.

However, this is to the detriment of induced drag F_{Di} and lift-to-drag ratio F_L/F_{Di}, increasing the former by up to 33.3 % and consequently decreasing the latter by up to 25.0 %.

Despite this increase, moment of induced drag M_{Di} drops by up to 32.8 %. Similar to variable span evaluation, the majority of the decrease occurs for ι between 0 and 0.7, exhibit relatively minor changes thereafter with lowest values between 0.8 and 0.9 and experience a slight increase up to 1.0.

4 DISCUSSION

Cubic span-loads entail relatively minor modifications to the shape of span-wise circulation distributions, yet their effect on wing moments, primarily of induced drag, is substantial. No investigated solution is purely beneficial, providing either lower force as well as moment of induced drag at the cost of increased span or reducing moments of lift and of induced drag while incurring drag penalties.

Since induced drag is of paramount concern to lifting surfaces, making increases thereof detrimental, the use of cubic distributions for wings of given span is unattractive. Such a conclusion should come as no surprise, since it is affirmation of long-standing knowledge [1]. Thus, results for variable span based of subsection 3.1 are discussed with respect to lifting surface applications.

Moments are of greater importance than forces for rotating wings, so that decreases in both moment of lift and of induced drag observed for constrained span benefit rotor blades, even in light of associated increases in induced drag. Implications of cubic distributions for given span evaluated in subsection 3.2 are analysed with respect to rotating systems, specifically rotor blades.

The general trend is that raising distribution factor ι provides diminishing returns, with the majority of improvements available for factors up to 0.6 to 0.8,

while drawbacks tend to expedite at higher values. For practical implementations, the best solution may therefore be in this range rather than a straight choice between the extremes of elliptic and bell-shaped.

The deduction of unidirectional circulation causing bidirectional trailing edge flow for a range of distribution factors is a systematic consequence of lifting-line theory, a result originally published by one of its authors [2], and leads to regions of negative induced drag. Since sign indicates orientation in the coordinate system, this result denotes forward acting force and can be interpreted as induced thrust [4], perhaps better designated induced propulsion due to its passive nature, although some disagree with such interpretation in conjunction with wing tip devices [9].

4.1 Variable span - lifting surfaces

For lifting surfaces, relevant relationships to be considered are increasing span, constant lift, negligibly changing moment of lift and decreasing induced drag and moment of induced drag as distribution factor ι is raised.

Constant lift together with negligible change in its moment mean that the span increases of up to 22.5 % involve elongation of a lifting surface while maintaining wetted area and structural strength, so that no viscous drag or weight penalties are incurred. Therefore, cubic distributions do not significantly impact characteristics, whether beneficially or detrimentally, besides those treated here.

Cubic span-loads reduce induced drag by up to 11.1 % with most of the drop occurring for ι up to 0.6. Indeed, together with span increases of 6.1 to 10.2 % for ι of 0.4 to 0.6, these results correspond to improvements observed for wing tip devices [9, 10, 11, 12] when treating height of vertical variants as span extensions. Moreover, outboard regions of upward flow correspond to negative incidence angles for winglets [13]. While these correlations confirm that the theory describes real effects with reasonable accuracy, it also shows that cubic distributions promise little induced drag enhancement beyond what is currently available.

The largest, and as yet largely unexplored, consequence lies with the effect that cubic distributions have on moment of induced drag. Total values for one semi-span are reduced by up to 44 %, with most of the decrease occurring for distribution factors up to 0.7. Structurally, this decreases horizontal loading and allows for lighter wing construction, though this benefit is counteracted in the case of wing-mounted engines that require structural strength to transfer thrust to the aircraft.

In terms of aerodynamic characteristics, lower moments of induced drag provide greater yaw stability, especially under asymmetric conditions such as cross-wind. For flight control, the yawing moments necessary for directional flight control are reduced, decreasing size or deflection of control surfaces.

Distributions with ι greater than 0.4 exhibit negative induced drag and associated moment in outboard segments for which lift is positive. Thus, these wing sections experience upward acting lift as well as forward acting force, interpretable as induced propulsion. Roll control surfaces placed in these sections provide direct coupling between the two as well as their associated moments, generating proverse yaw as proposed and experimentally observed by [4]. As such, the results herein present theoretical confirmation of this effect as well as the means for further investigation and optimisation.

Due to diminishing returns as it is raised, ideal values of ι for implementing lifting surfaces with proverse yaw are estimated to be 0.7 to 0.8. For these, outboard regions of negative moments of induced drag depicted in Figure 5 are of similar area and peak magnitude than for larger factors, making their roll-to-yaw coupling similar. Moreover, induced drag is reduced by 10.6 to 10.9 %, only slightly below the maximum reduction of 11.1 %, and moment of induced drag by 39.0 to 41.7 %, also just shy of the peak value of 44.0 %. The vast majority of improvement is then accessible for span extensions of 12.7 to 15.5 %, significantly below the maximum of 22.5 %.

Practical implementations for lifting surfaces necessitate span-wise twist to generate appropriate circulation distributions, resulting in varying pitch moments in proportion to trailing edge vertical flow velocities depicted in Figure 3. Inboard downwash regions exhibit nose-down while outboard upwash ones experience nose-up pitch moments, counteracting each other and reducing the sum value. In addition, control surfaces in either section are furnished with according characteristics, providing the ability to modify pitch bidirectionally. Together, they benefit lifting surfaces by reducing or potentially removing necessity of dedicated horizontal stabilisers and elevators.

The combination of proverse yaw and varying pitch moments alleviates several challenges in designing tailless aircraft [14] as well as providing a basis for explaining controlled flight of birds without vertical and with no or comparatively small horizontal tails [4]. Accessing these benefits requires span extensions and is therefore only viable in applications where such a choice is possible.

4.2 Given span - rotor blades

The relationships considered more relevant to rotating systems are constant lift and span, increasing induced drag and decreasing moment of lift and of induced drag when distribution factor ι is raised, as presented in subsection 3.2. Results of Table 3 show ap-

preciable reductions up to 20.0 % and 32.8 % in moments of lift and of induced drag, respectively, while increasing induced drag by up to 33.3 %. However, the range of 0.7 to 0.9 for ι is most appealing, since moment of induced drag is close to its minimum therein with little variation, as evident in Figure 7, while induced drag remains substantially below its maximum increase at 13.5 to 25.3 %.

Conventional rotor optimisation is predicated on minimising wake energy, which is achieved through accelerating fluid by constant velocity across a rotor area [5, 15]. Each blade is designed to generate span-wise constant downwash, which makes the situation analogous to that of elliptic circulation distribution for lifting surfaces. Consequently, such designs exhibit flow velocity discontinuities at blade tips that generate significant noise.

Both moment of lift and of induced drag contribute to the moment of a rotor shaft. Aforementioned reductions indicate that optimising rotor blades for minimal moment rather than wake energy may produce significant reductions in shaft power, the product of rotary moment and angular velocity. Systems converting shaft power into flow, such as fans, propellers or helicopter rotors, stand to benefit whereas it is detrimental to power generation applications, e.g. gas, steam, water or wind turbines. Indeed, results for the elliptic distribution support the notion that for the latter case, the approach of minimising wake energy is very likely the best strategy, since it describes their intended function.

The theory developed herein is based on span-wise constant free-stream flow in the plane of a lifting surface, as depicted in Figure 1. The situation for rotor blades differs in three main aspects, so that these models need to be extended to cover these deviations.

The first is to incorporate span-wise variable free-flow velocity, since blade incident flow depends on rotational speed and distance to the axis of revolution, being smaller towards the centre and greater towards the perimeter. To achieve lower moments of induced drag, cubic distributions concentrate circulation and trailing edge vertical flow closer to the wing centreline while lowering them in outer regions. These two characteristics run contrary to each other so that the anticipated outcome of span-wise variable free-flow is for reductions in moments to be diminished.

Moreover, the theory must be expanded to include centreline offsets. Rotors require hubs to which their blades are attached, furnishing them with an offset distance to the axis of rotation that is necessary to translate rotational speed into flow velocity. Simultaneous increase in induced drag and decrease in moment of lift and of induced drag mean that the former diminishes benefits of the latter once an offset is added. In the majority of applications, rotor blade spans are significantly larger than hub diameters, so that the advantages of lower moments prevail and cubic distributions are expected to predominantly reduce shaft power, though advantages are expected to be below those presented here.

Thirdly, the theory needs to be extended to account for impact of blade pitch resulting from flow perpendicular to the plane of rotation, due to wash of preceding blades as well as advance motion of the rotor. Blades are set into oncoming flow in order to function as foils effectively, creating angles between lift generated by blades and the desired direction of thrust. The greater these angles, the lower the beneficial portion of lift and the larger its detrimental contribution to rotary moment. This effect is particularly pronounced on inner blade sections where flow due to rotation is low as well as on aircraft traveling at high velocities for which advance motion is comparatively large in relation to rotational speeds. As such, this runs contrary to cubic distributions raising circulation and flow towards the root while decreasing it towards the perimeter and is thus expected to diminish benefits further.

Overall, a reduction is expected to remain since reductions of 15% are purported with an approach focused on moments rather than wake energy using a different distribution [16]. The general nature of the theory derived herein implores further exploration, both theoretically and practically, for both aerodynamic and hydrodynamic applications seeking to convert shaft power into flow.

A further, and potentially more appealing, effect lies with the reduction or elimination of tip velocity discontinuities observed for cubic distributions in Figure 3. Since distribution factors of 0.7 to 0.9 present the most appealing results for given span in Table 3 and their outer upwash sections experience no abrupt discontinuity, these evaluations predict corresponding reduction or elimination of tip noise generation in aerodynamic as well as cavitation in hydrodynamic applications.

5 CONCLUSION

Lifting-line theory for circulation distributions proposed in [2] and termed cubic herein has been extended to moments of force for lift and induced drag. Evaluation with span-wise constant free-low have been performed for distribution factors of 0 to 1.0 in 0.1 steps when constraining integrated moment of lift as per original publication as well as for given span. Both constraints give rise to appreciable reductions in moments as distribution factor is raised with returns diminishing as the maximum value of 1.0 is approached.

Implications for constrained integrated moment of lift are more relevant to lifting surfaces. Observed re-

ductions in induced drag at the expense of increased span are in reasonable agreement with effects of wing tip devices. The impact on moment of induced drag is greater, reducing yawing moments to be overcome by control surfaces for directional flight and lowering susceptibility to unsteady flow conditions. Moreover, regions of negative induced drag and associated moment are ascertained in outboard sections, thereby aligning roll and yaw moments as needed for banking turns and providing theoretical confirmation of proverse yaw observed experimentally in literature. Together, these two effects open up the possibility of directional flight without auxiliary yaw devices.

Implementing such distributions involves span-wise wing twist, reducing pitching moments as well as lessening demands on horizontal stabilisers and elevators. In combination with aforementioned yaw characteristics, this provides explanations for the readily observable controlled flight of birds and predicts advantages for tailless aircraft design. The necessity of extending wing spans to achieve these benefits limits its application to lifting surface implementations where such a choice is feasible.

Evaluation for constrained span is of more pertinent interest to rotor blades, equivalent to maintaining rotor area, and results show contrasting trends of increasing induced drag and decreasing moment of lift and of induced drag as the distribution factor is raised. The latter two contribute to shaft power, so that reductions correlate directly. Therefore, cubic distributions may offer substantial benefits to rotor designs when optimising for shaft power rather than wake energy, as is the current norm. Since moments are consistently reduced, only applications seeking to convert shaft power into flow and associated forces stand to benefit while power generators suffer performance losses.

A further ramification is the reduction or elimination of flow velocity discontinuities at the tips predicting corresponding impacts on noise generation. For driven rotors, blade tip noise represents a major issue so that applying cubic distributions offers the potential to address its root cause, the most desirable form of abatement. In addition, cavitation in hydrodynamic propellers is expected to be similarly influenced.

To investigate the proposed improvements to rotors, theoretical derivations presented herein need to be adapted to span-wise varying flow, expanded to consider centreline offsets due to rotor hubs and include the impact of blade pitch to the desired direction of action. All three aspects are expected to degrade improvements compared to results presented herein and experimental investigations are needed to assess effectiveness in practical implementations. The dual purported benefits of reduced shaft power and noise generation are of too great an appeal to driven rotors to ignore in light of the scope of eventual applications to both airborne and maritime vehicles.

The accuracy of all these theoretical predictions is limited by simplifications made in the derivation of lifting line theory, though it has established itself to be reasonably reliable in its predictions. The observation that unidirectional circulation produces bidirectional trailing edge vertical flow leads to horizontal forces acting in both forward and aft directions and thus generates induced drag as well as, for lack of a better term, propulsion. Being in agreement with as yet singularly reported experimental data, this finding encourages further exploration of the topic.

Contact email:

dominic@pearman.biz

Symbols

F_L	lift	N
F_{Di}	induced drag	N
M_L	moment of lift	N m
M_{Di}	moment of induced drag	N m
Γ	circulation	m^2/s
Γ_0	central circulation	m^2/s
F_L/F_{Di}	lift-to-drag ratio	
ι	circulation distribution factor	
ρ	density	g/m^3
ξ	relative span position	
b	span	m
b_e	span of elliptic distribution	m
r_{IM}	radius of integrated moment	m
v	velocity	m/s
v_z	trailing edge vertical flow velocity	m/s

References

[1] L. Prandtl. “Tragflügeltheorie. I. Mitteilung.” In: *Nachrichten der K. Gesellschaft der Wissenschaften zu Göttingen* (1918), pp. 451–477.

[2] L. Prandtl. “Über Tragflügel kleinsten induzierten Widerstands”. In: *Zeitschrift für Flugtechnik und Motorluftschiffahrt* 24 (1933), pp. 556–561.

[3] R. Jones. *The spanwise distribution of lift for minimum induced drag of wings having a given lift and a given bending moment*. Tech. rep. 2249. National Advisory Committee for Aeronautics, Dec. 1950.

[4] A. Bowers et al. *On Wings of the Minimum Induced Drag: Spanload Implications for Aircraft and Birds*. Tech. rep. TP-2016-219072. National Aeronautics and Space Administration, Mar. 2016.

[5] A. Betz. “Schraubenpropellor mit geringstem Energieverlust”. In: *Nachrichten der K. Gesellschaft der Wissenschaften zu Göttingen* (1919), pp. 193–217.

[6] S. Goldstein. “On the Vortex Theory of Screw Propellers”. In: vol. 123. Proceedings of the Royal Society London A. 1929.

[7] G. van Rossum. *Python tutorial*. Tech. rep. CS-R9526. Centrum voor Wiskunde en Informatica, May 1995.

[8] Aaron Meurer et al. “SymPy: symbolic computing in Python”. In: *PeerJ Computer Science* 3 (Jan. 2017), e103. DOI: 10.7717/peerj-cs.103.

[9] D. McLean. “Wingtip Devices: What They Do and How They Do It”. In: Performance and Flight Operations Engineering Conference. Boeing. 2005.

[10] R. Jones and T. Lasinski. *Effects of Winglets on the Induced Drag of Ideal Wing Shapes*. Tech. rep. NASA TM-81230. National Aeronautics and Space Administration, 1980.

[11] National Research Council. *Assessment of Wingtip Modifications to Increase the Fuel Efficiency of Air Force Aircraft*. The National Academies Press, 2007.

[12] D. Scholz. “Definition and discussion of the intrinsic efficiency of winglets”. In: Aerospace Europe CEAS 2017 Conference. Oct. 2017.

[13] R. Whitcomb. *A Design Approach and Selected Wind-Tunnel Results at High Subsonic Speeds for Wing-Tip Mounted Winglets*. Tech. rep. TN D-8620. National Aeronautics and Space Administration, July 1976.

[14] K. Nickel and M. Wohlfahrt. *Schwanzlose Flugzeuge*. Birkhäuser Verlag, 1990.

[15] W. Nelson. *Airplane Propellor Principles*. John Wiley & Sons Inc., 1948.

[16] A. Bowers and E. Uden. *Propellor design*. United States Patent 10,414,485. Aug. 2019.